

Final Draft
of the original manuscript:

Hiebl, B.; Ascher, L.; Luetzow, K.; Kratz, K.; Gruber, C.; Mrowietz, C.;
Nehring, M.E.; Lendlein, A.; Franke, R.-P.; Jung, F.:

**Albumin solder covalently bound to a polymer membrane:
New approach to improve binding strength in laser tissue
soldering in-vitro**

In: Clinical Hemorheology and Microcirculation (2018) IOS Press

DOI: 10.3233/CH-189108

1 **Albumin solder covalently bound to a polymer membrane: new approach to improve**
2 **binding strength in laser tissue soldering *in-vitro***

3
4 B. Hiebl^{1,2}, L. Ascher^{2,3}, K. Luetzow², K. Kratz², C. Gruber¹, C. Mrowietz^{2,4}, M.E. Nehring¹, A.
5 Lendlein², R.-P. Franke⁵ and F. Jung²

6
7 1: Institute for Animal Hygiene, Animal Welfare and Farm Animal Behaviour and Virtual Center for
8 Replacement – Complementary Methods to Animal Testing, University of Veterinary Medicine
9 Hannover, Foundation, Hannover, Germany

10 2: Institute of Biomaterial Science and Berlin-Brandenburg Center for Regenerative Therapies,
11 Helmholtz-Zentrum Geesthacht, Teltow, Germany

12 3: BAM Federal Institute for Materials Research and Testing, Berlin, Germany

13 4: Institute for Clinical Hemorheology and Transfusion Medicine, University of Saarland,
14 Homburg/Saar, Germany

15 5: Central Institute for Biomaterials, University of Ulm, Ulm, Germany

16
17
18 Corresponding author: Prof. Dr. Bernhard Hiebl, Bernhard.hiebl@tiho-hannover.de

19
20 **ABSTRACT**

21 Laser tissue soldering (LTS) based on indocyanine green (ICG)-mediated heat-denaturation of
22 proteins might be a promising alternative technique for micro-suturing, but up to now the problem
23 of too weak shear strength of the solder welds in comparison to sutures is not solved. Earlier
24 reports gave promising results showing that solder supported by carrier materials can enhance the
25 cohesive strength of the liquid solder. In these studies, the solder was applied to the carriers by dip
26 coating. Higher reliability of the connection between the solder and the carrier material is expected
27 when the solder is bound covalently to the carrier material. In the present study a poly(ether imide)
28 (PEI) membrane served as carrier material and ICG-supplemented albumin as solder substrate.
29 The latter was covalently coupled to the carrier membrane under physiological conditions to
30 prevent structural protein changes. As laser source a diode continuous-wave laser emitting at 808
31 nm with intensities between 250 mW and 1500 mW was utilized. The albumin functionalized carrier
32 membrane was placed onto the tunica media of explanted pig thoracic aortae forming an
33 overlapping area of approximately $0.5 \times 0.5 \text{ cm}^2$. All tests were performed in a dry state to prevent
34 laser light absorption by water. Infrared spectroscopy, spectro-photometrical determination of the
35 secondary and primary amine groups after acid orange II staining, contact angle measurements,
36 and atomic force microscopy proved the successful functionalization of the PEI membrane with
37 albumin. A laser power of 450 mW LTS could generate a membrane-blood vessel connection
38 which was characterized by a shear strength of $0.08 \pm 0.002 \text{ MPa}$, corresponding to 15% of the

39 tensile strength of the native blood vessel. Theoretically, an overlapping zone of 4.1 mm around
40 the entire circumference of the blood vessel could have provided shear strength of the PEI-
41 membrane-blood vessel compound identical to the tensile strength of the native blood vessel.
42 These *in-vitro* results confirmed the beneficial effects of solder reinforcement by carrier
43 membranes, and suggest LTS with covalently bound solders on PEI substrates for further studies
44 in animal models.

45

46 **Keywords** Laser tissue soldering, blood vessel anastomosis, laser welding, solder carrier,
47 poly(ether imide) membrane

48

49

50

51 1. INTRODUCTION

52 Micro-suturing is the gold standard for small blood vessel anastomosis. But this suturing procedure
53 is time consuming and associated with an increasing risk of hypoxia and tissue damage, because
54 during the suturing process the blood flow through the target vessel and the supply of the vessel
55 with oxygenated blood, respectively, are stopped. Additionally, the quality of micro-suturing strongly
56 depends on the skills of the surgeon. Various methods other than conventional suturing such as
57 rings, clips, adhesives, and laser tissue fusion have been developed [1]. Among these methods,
58 the laser assisted methods like laser tissue soldering (LTS) have more advantages and lower risks
59 of stenosis and foreign body reactions since they require shorter time for surgery, are less
60 traumatic to the surrounding tissues and limit anastomotic thrombogenicity [2]. Different laser light
61 sources (CO₂-, argon-, diode-lasers) are in use, where the diode laser is the most popular at
62 present. Typically, for tissue welding, deeply penetrating diode lasers (emitting at 800-810 nm) are
63 used, in combination with a strong chromophore-enhanced protein solder containing the dye ICG.
64 ICG has a maximum absorption coefficient at 805 nm and binds preferentially to proteins [3]. ICG
65 mediates absorption of the laser light and resulting thermal effects can contribute essentially to the
66 fusion of local tissues.

67 Laser-soldered anastomoses form an immediate watertight connection. Furthermore, it has been
68 shown that laser-soldered wounds have a better inflammatory response than sutured wounds [4-6].
69 One of the major drawbacks of LTS is the weak shear strength of the solder welds when compared
70 to sutures. Earlier reports showed that carrier materials like poly[(DL-lactic acid)-co-(glycolic acid)]
71 (PLGA) or poly-(ϵ -caprolactone) can reinforce cohesive strength of the liquid solder [7, 8]. The
72 carrier substrates enhanced the physical strength and prevented a draining of the liquid solder and
73 a leakage of the solder into intraluminal spaces resulting in embolism [9]. Up to now the solders
74 were applied to the carrier surfaces by dip coating [8]. However, in these studies the solder
75 coagulum itself became the limiting factor in the strength of the repair [8]. This motivated the study
76 presented here, to apply LTS with a solder covalently bound to a carrier membrane. The latter was

77 made of poly(ether imide) (PEI) which can be steam sterilized and the membranes show good
78 biocompatibility [10]. Such membranes can be covalently modified i.e. with amino-functionalized
79 macromolecules, which react with the imide repeating group in the main chain of PEI [11, 12].
80 Additionally, the absorption coefficient of PEI at a wavelength of 808 nm, used for LTS in this study,
81 is low ($< 1 \text{ cm}^{-1}$) [13]. Thus the laser light is only minimally attenuated by the PEI membrane.

82
83

84 **2. MATERIALS and METHODS**

85 **2.1 Membrane**

86 PEI (Ultem 1000, GE-Plastics, Fairfield, USA) flat sheet membranes were prepared by a
87 continuous non-solvent induced phase inversion process using a solution of 17.5 wt.% PEI in 30
88 wt.% γ -butyrolactone and 52.5 wt.% dimethylacetamide and water as a coagulant. Membranes
89 were prepared both on a polyester nonwoven support and as free-standing membrane.

90

91 **2.2 Surface functionalization**

92 PEI membranes were functionalized with albumin fraction V from bovine serum (MERCK,
93 Germany) to provide a solder. Based on wet chemistry, the carbonyl groups of the imide backbone
94 part of PEI were coupled with amine groups of the albumin. For this amination process the PEI
95 membrane was incubated in a 2 wt.% aqueous solution of albumin in PBS (pH 7.4; ratio 1:1) at
96 40°C for 2, 5, 10, 30, 60, 180, 480, or 960 min. Functionalized membranes were thoroughly
97 washed in phosphate-buffered saline (PBS) containing 150 mM NaCl, 5.8 mM $\text{NaH}_2\text{PO}_4 \cdot \text{H}_2\text{O}$, and
98 5.8 mM $\text{Na}_2\text{HPO}_4 \cdot 12\text{H}_2\text{O}$ (pH 7.4; Sigma Aldrich, Germany) and then stored in the wet state at 4°C
99 until further investigations.

100

101 **2.3 Characterization**

102 Tests for surface characterization with the exception of the acid orange II assay were performed
103 after stabilization of the backside of the carrier membrane with a polyester fleece (Histar 100, GMT,
104 Germany).

105 Functionalization of membranes on the non-woven support were analyzed by Fourier transform
106 attenuated total internal reflection infrared (FT-ATR-IR) spectroscopy (Nicolet MagnaIR™ 550,
107 Thermo Fisher Scientific, Waltham, MA, USA). All spectra were normalized to the C-O stretching
108 vibration of the ether bond at 1230 cm^{-1} .

109 The functionalization of free-standing membranes, which leads to an increase of primary and
110 secondary amine groups on the membrane surface, was evaluated with an acid orange II assay
111 [14]. The modified membrane was washed three times with 2 ml of dilute hydrochloric acid (pH 3)
112 for 10 minutes to protonate all the amines. Subsequently, it was incubated in a 500 μM acid orange
113 II solution (pH 3 adjusted with HCl) for 24 h at room temperature. Thereafter, the membrane was
114 washed again three times with diluted hydrochloric acid (pH 3) for 10 minutes until the solution was

115 colorless. With diluted sodium hydroxide solution (pH 12), the dye was again washed off by
116 deprotonation of the amines from the membrane. The optical density of the solution was measured
117 spectrophotometrically at 492 nm (SpektraFluor Plus, Tecan, Switzerland). The amount of amine
118 groups on the membrane surface was determined by comparison with a standard curve of known
119 concentrations of acid orange II. The assay was performed directly after PEI functionalization with
120 albumin and also after desorption of the non-covalently bound albumin from the PEI membrane
121 applying the detergent SDS (0.3 M NaOH/1% SDS) for 1 h at room temperature under continuous
122 shaking.

123 Contact angle measurements based on the captive bubble method were performed on supported
124 membranes to assess membrane wettability and hydrophobicity respectively. For these tests a
125 drop shape analyzer (DSA 100) from Krüss GmbH (Hamburg, Germany) was used.

126 Surface topography of the supported PEI membranes was characterized by using atomic force
127 microscopy (AFM, tapping mode; NanoScope, MultiMode V, Bruker Nano, Germany). Only wet
128 membranes were used which were incubated in PBS without calcium and magnesium ions at pH
129 7.4. The scanning area for each scan was 10.0 μm^2 and the mean square roughness (R_q) was
130 determined by analyzing three samples at three different areas.

131

132 **2.4 Tissue preparation**

133 Thoracic aortas were obtained from pigs, which were sacrificed at the Charité-University Medicine
134 Berlin, Research facilities for Experimental Medicine, Germany, in the context of animal
135 experiments according to an approved study (LAGESO: **AZ G 0298/07**). The aortas were rinsed
136 with PBS, wrapped in saline soaked gauze, and stored at 4°C until required. Before usage, aortas
137 were cut into rectangular specimens having approximate dimensions of 0.5 × 2 cm². Of each
138 specimen the adventitia was stripped and the tunica media was trimmed to obtain a specimen
139 thickness of approximately 1 mm.

140

141 **2.5 Laserwelding**

142 For near-infrared laser welding, the albumin coating was supplemented with the photosensitizer
143 ICG. Therefore the albumin-functionalized free-standing PEI membranes were incubated for 12 h in
144 an aqueous solution containing 0.02 mg·ml⁻¹ indocyanine green (ICG, Sigma Aldrich, Germany).
145 After this period, the PEI membrane was rinsed twice with PBS to remove unbound ICG from the
146 surface. Based on the concentration of the unbound ICG in the rinsing solution, the concentration
147 of ICG bound to the PEI membrane was calculated to be 2.8 $\mu\text{g}\cdot\text{cm}^{-2}$. The functionalized
148 membrane was air-dried before usage to limit laser absorption by water [4, 15].

149 A continuous wave diode laser emitting at 808 nm (Albers Laser GmbH, Germany) was used as
150 light source. Laser radiation was delivered through a 190- μm -core silica fiber. Each fiber
151 terminated in a hand piece, which enabled easy and precise handling. As operating diode power
152 250, 350, 450, 650, 850, 1050, 1250, 1450, or 1500 mW were applied.

153 Specimens with a size of $0.5 \times 2.0 \text{ cm}^2$ were cut from the membranes and placed onto the media
154 of the blood vessels which were blotted before with cotton gauze to remove excess moisture. The
155 overlapping area between the PEI membrane and the blood vessel had a size of approximately 0.5
156 $\times 0.5 \text{ cm}^2$. The laser beam was evenly guided via a handpiece in a meandering way over the
157 entire non-coated surface of the PEI membrane within 30 sec, maintaining a 90° angle between
158 the beam and the membrane. A distance holder on the handpiece guaranteed a constant distance
159 of 3.0 mm between the fiber tip of the handpiece and the membrane surface. Non-functionalized
160 PEI membranes and functionalized PEI membrane after denaturation of the albumin layer at 80°C
161 served as negative controls.

162

163 **2.6 Shear strength analysis**

164 Shear strength measurements of the resulting PEI membrane-blood vessel connections were
165 carried out on an Instron 3345 shear tester, (Instron GmbH, Darmstadt, Germany). The membrane-
166 blood vessel-compound was fixed in the apparatus by the distal ends of the membrane and the
167 blood vessel which were outside the overlapping area of both and not connected together by
168 welding. Tests were performed at room temperature at a strain velocity of 10 mm min^{-1} until the
169 polymer-tissue-compound disintegrated.

170

171 **2.7 Histology**

172 Immediately after finishing the laser welding process the membrane-blood vessel compounds were
173 embedded in section medium (Neg-50, Thermo Scientific, Germany) and subjected to frozen
174 sectioning. For assessment of tissue structural integrity, eight sections with a thickness of $4 \mu\text{m}$
175 were made from each compound and hematoxylin-eosin (HE) stained according to the protocol of
176 Romeis [16]. For dehydration and conservation respectively, the stained specimens were
177 immersed in 70 vol% ethanol, 96 vol% ethanol, 100% ethanol, and Roti[®]-Histol (1.5 min each). All
178 sections were finally mounted in Roti[®] Histokitt II (Carl Roth, Germany) on glass slides before
179 analysis by transmitted light microscopy (phase contrast mode). Each slide was evaluated at five
180 different fields of view using the image analysis software AxioVisio (Zeiss, Germany).

181

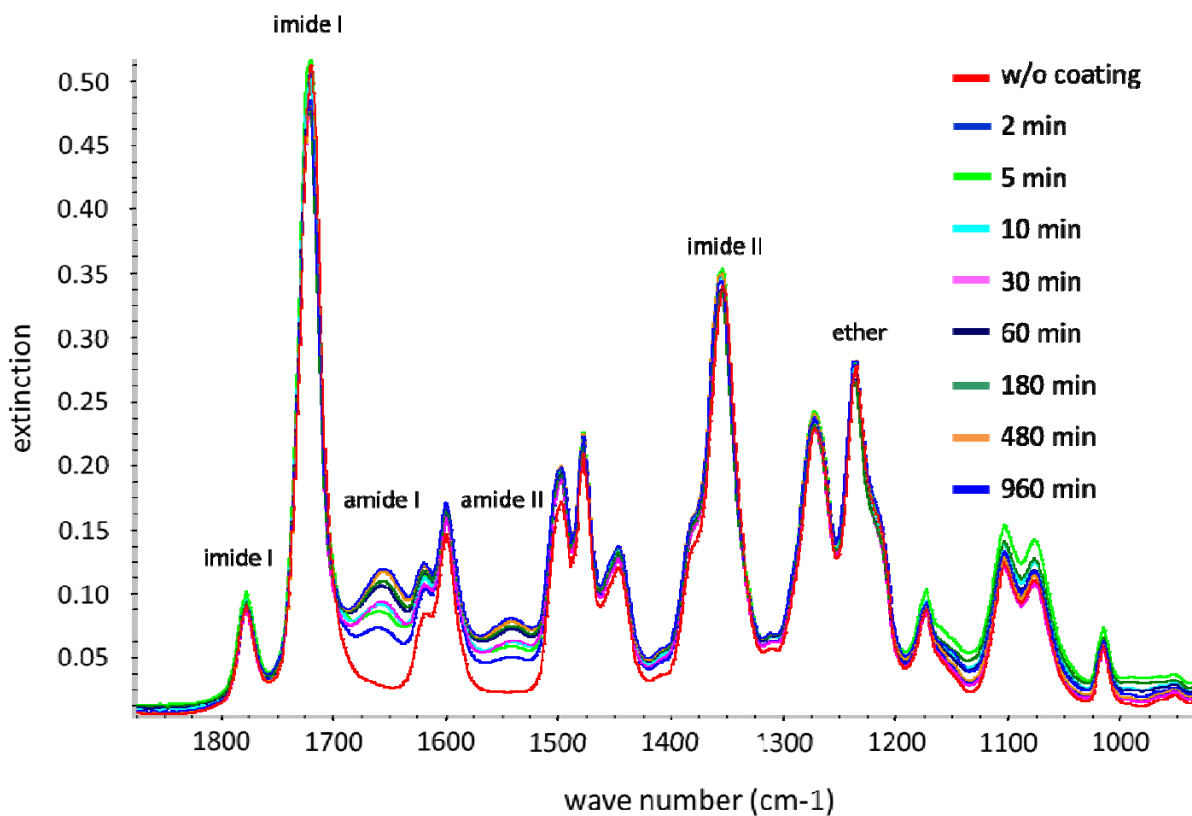
182

183 **3. RESULTS**

184 **3.1 Surface functionalization**

185 In the FT-ATR-IR spectrum of the albumin functionalized PEI membrane symmetric and
186 asymmetric C=O stretching vibration of the imide group caused strong absorption bands at 1720
187 and 1780 cm^{-1} (see Fig. 1). At 1360 cm^{-1} the C-N stretching vibration of the imide was detectable.

188



189
190

191 **Figure 1:** FT-ATR-IR spectra of a PEI membrane before (red colored line) and after albumin
192 functionalization at different functionalization times (2 to 960 min) carried out at pH 7.4 and 40°C.

193

194 Functionalization with albumin led to an increase of the amide I-band (C=O stretching vibration) at
195 1660 cm⁻¹ and of the amide II-band (C-N stretching vibration) at 1560 cm⁻¹; the longer the reaction
196 time (2 to 960 min) the stronger the increase.

197 PEI membrane functionalization for 960 min with albumin resulted in an amine content on the
198 membrane surface of 175.7 ± 7.2 nmol·cm² (n = 6) which was 5.7-fold higher than without the
199 albumin coating (31.0 ± 3.4 nmol·cm², n = 6). After desorption of the non-covalently bound albumin
200 from the PEI membrane by using the detergent SDS (0.3 M NaOH/mol, 1% SDS), 171.4 ± 5.1
201 nmol·cm⁻² (n = 6) of the amines were left equivalent to a 2.5% reduction.

202

203 3.2 Surface wettability

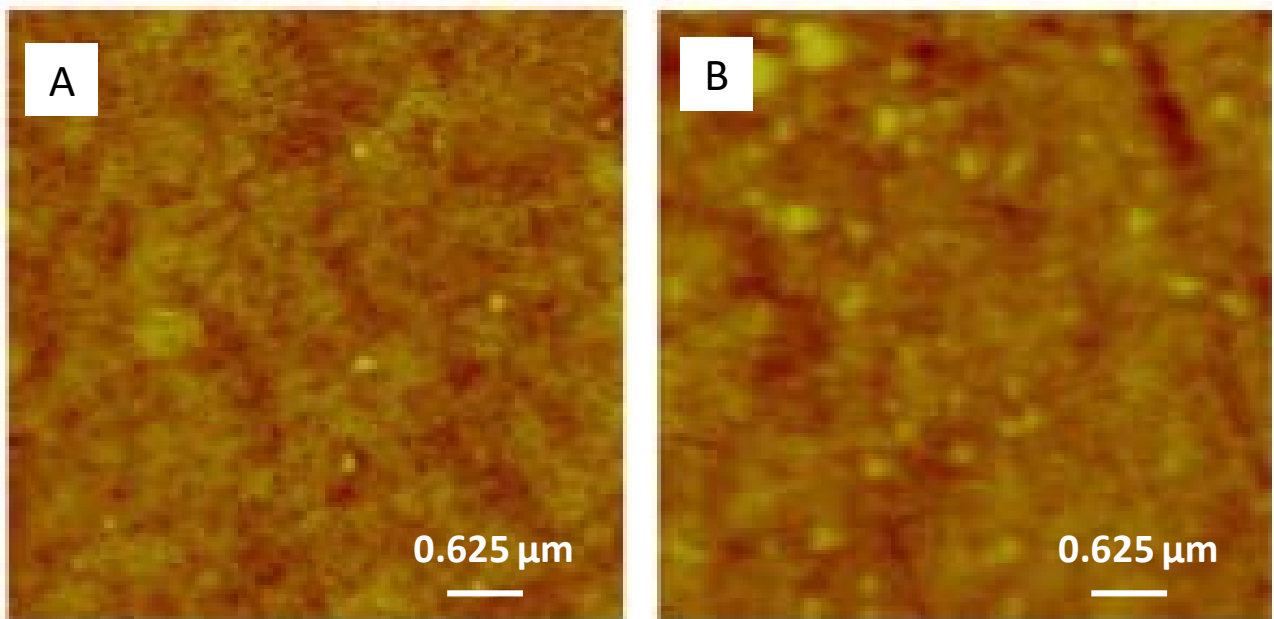
204 The advancing and receding contact angles (θ_{adv} and θ_{rec}) were 61.9 ± 4.8° and 32.2 ± 1.0° on the
205 non-functionalized PEI membrane. PEI functionalization resulted in a significant decrease of the
206 contact angle to θ_{adv} = 31.5 ± 2.3° and θ_{rec} = 28.6 ± 1.3°. In accordance, the calculated hysteresis
207 on the non-functionalized PEI was 29.7° and significantly higher than after functionalization with
208 albumin (3.0°).

209

210 3.3 Surface roughness

211 The non-functionalized PEI membrane exhibited an almost homogenous surface topography

212 characterized by a mean root mean square roughness of $R_q = 6.47$ nm (n=9). Surface
213 functionalization resulted in an increased R_q value of 9.92 nm (n=9) showing a more
214 heterogeneous surface topography (Fig. 2).
215



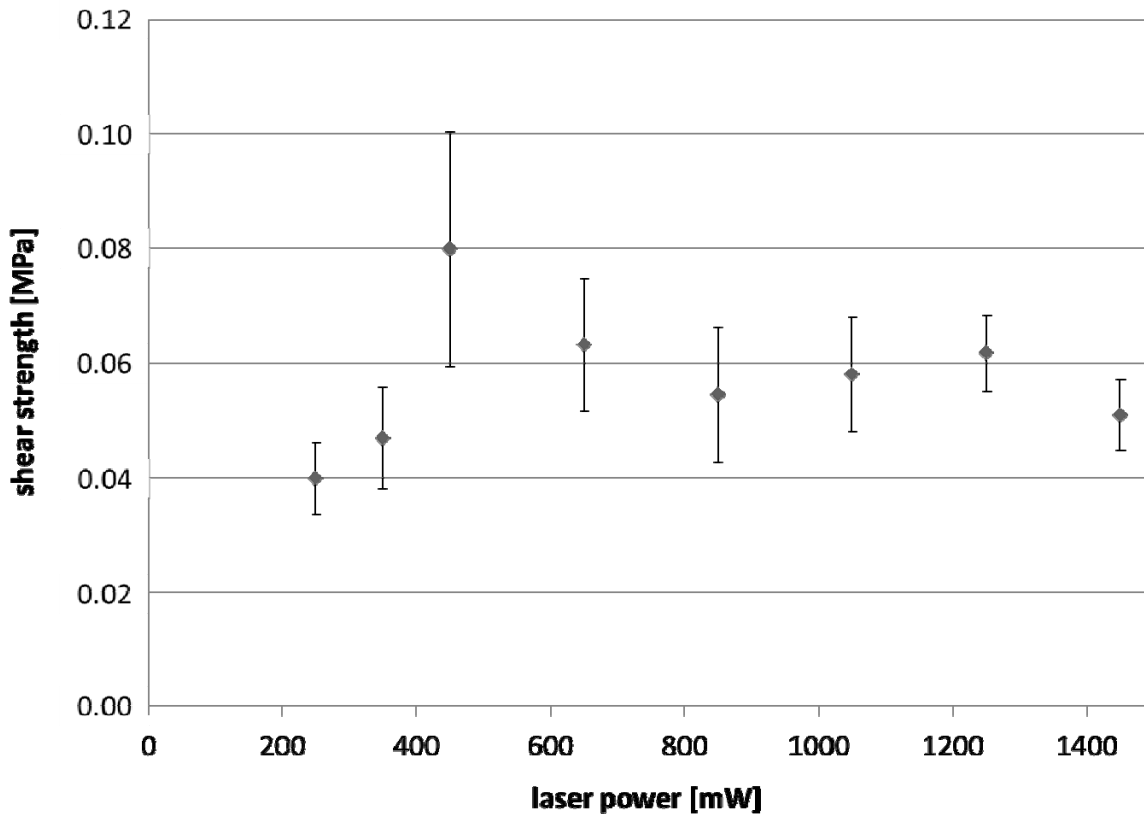
216
217 **Figure 2:** Surface roughness measured by Atomic Force Microscopy (AFM) of a PEI membrane
218 (A) before and (B) after albumin functionalization at pH 7.4 and 40 °C for 960 min. Brightness
219 increased with increasing height (roughness); maximal height: 150 nm, n = 9.

220

221 **3.4 Testing of Shear Strength**

222 Shear strength of PEI-blood vessel compounds (connecting area of 0.25 cm²) was strongly
223 depending on the used power applied. At 250 mW the shear strength of the PEI-blood vessel
224 connection measured 0.04 ± 0.01 MPa. At a power of 450 mW the maximal shear strength ($0.08 \pm$
225 0.02 MPa) was reached (n = 7 each; Fig. 3). This shear strength corresponds to 11.4 - 22.2%
226 (mean 15.1%) of the tensile strength of the native thoracic artery (native artery: min: 0.36 MPa,
227 max: 0.70 MPa; mean: 0.53 ± 0.24 MPa, n = 10). The use of higher laser powers did not result in
228 higher shear strength. There was a decrease, rather, of the shear strength with laser powers
229 surpassing 450 mW.

230



231

232 **Figure 3:** Shear strength of functionalized PEI membrane-blood vessel compounds coupled to one
 233 another by laser welding with a continuous wave diode laser emitting at 808 nm at different laser
 234 powers; means and standard deviation, n = 7.

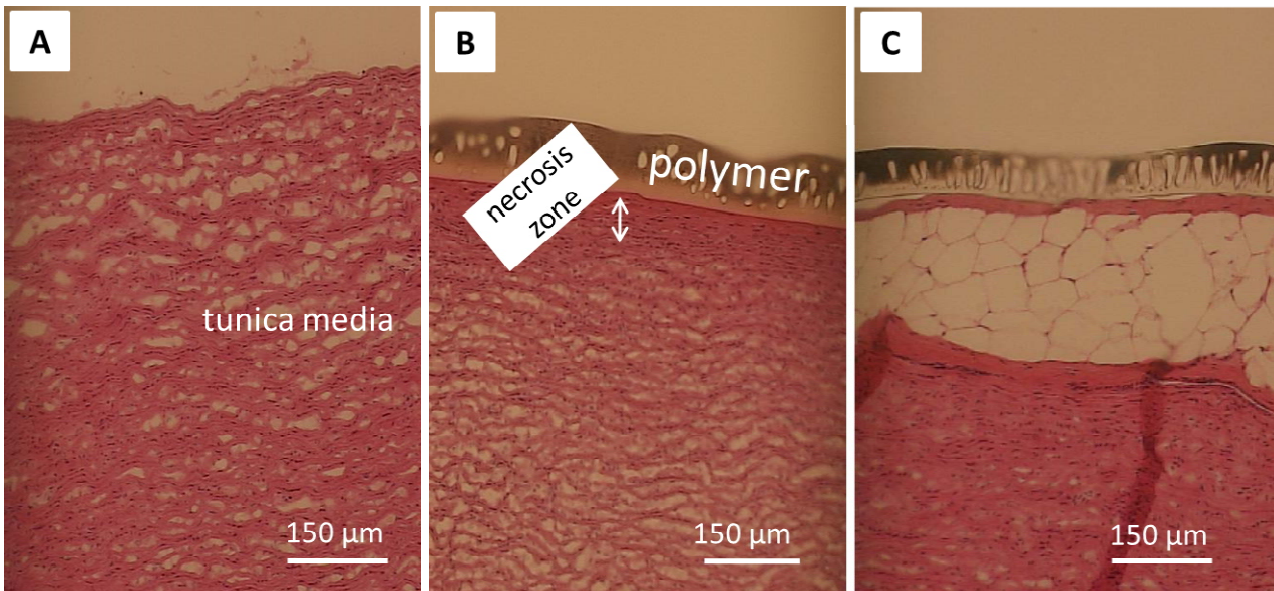
235

236 3.5 Histological findings

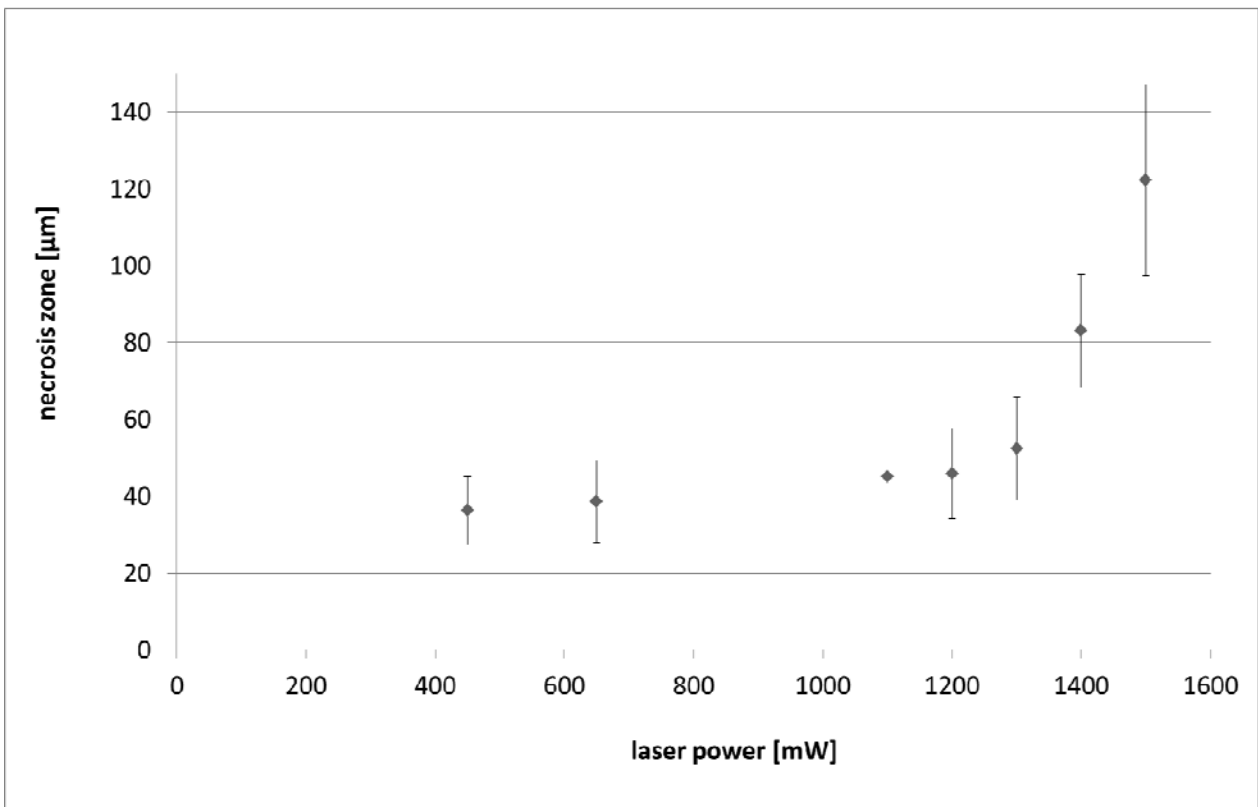
237 The peripheral tunica media of the blood vessels changed due to the laser soldering process to a
 238 compact eosinophilic necrosis zone with clearly delineated collagen fiber bundles. The
 239 organization of the collagen fibers in this zone changed remarkably and the number of cell nuclei
 240 was drastically reduced (Fig. 4).

241 Welding of the functionalized PEI membrane onto this dissected outer layer of the explanted pig
 242 aorta resulted in a more stable junction between both when the laser power did not exceed 450 mW
 243 (see Fig. 3). However, the outer layers of the tunica media were affected by the laser welding
 244 process, and a necrotic zone marked the interface between the PEI membrane and the blood
 245 vessel reaching from $36.4 \pm 9.0 \mu\text{m}$ at 450 mW up to 122.2 ± 24.8 at 1500 mW (n = 7 each; see
 246 Fig. 5). Laser powers higher than 450 mW additionally caused non-connected focal areas which
 247 increased in size with increasing laser power.

248



249
 250 **Figure 4:** Histology of pig aorta wall alterations induced by thermal effects of laser soldering; HE
 251 staining of the extraluminal part (tunica media) of the thoracic artery without treatment (A); after
 252 welding together with an albumin-functionalized PEI membrane using a continuous wave 808 nm
 253 diode laser with a laser power of 450 mW (B) or 1500 mW (C).
 254



255
 256 **Figure 5:** Necrosis zone of the outer tunica media after PEI-aorta junction generated by Laser
 257 welding using a continuous 808 nm diode laser with a laser power of 450-1500 mW; means and
 258 standard deviation, n = 7.
 259
 260

261 The PEI membrane itself with the characteristic finger pores was practically not affected by the
262 laser welding process. With increasing laser power the size and the number of finger pores
263 remained constant.

264

265

266 **4. DISCUSSION**

267 The conventional technique for blood vessel anastomosis is micro-suturing, which can cause clot
268 formation at the endoluminal perforation sites [1–5]. In addition, micro-suturing requires major
269 surgical skills and is often time consuming. Both aspects can adversely affect the therapeutic
270 success especially under clinical conditions where temporary ischemia is an issue for the survival
271 of anastomosed blood vessels. Another disadvantage of suturing is the necessity for the surgeon
272 to have free moving space which limits the practicability of this technique for minimally invasive
273 surgery. Laser tissue soldering (LTS) based on an ICG-mediated heat-denaturation of proteins
274 might be a promising alternative technique. However, one of the major drawbacks of LTS is the
275 weak shear strength of the solder welds when compared to sutures. In this study, it was tested
276 whether sufficient shear strength of the solder welds can be achieved by a carrier membrane to
277 which the chromophore-enhanced protein solder substrate is covalently bound and which can
278 provide additional physical strength to the weld. The membrane also prevents the ICG to spread
279 out over a large volume of tissue, thus failing to confine the welding procedure locally. Here the
280 support membrane was made of the polymer PEI because this polymer allows steam sterilization,
281 has shown good cell compatibility, and can be covalently functionalized through reaction of
282 nucleophiles with the imide group [10, 12].

283 The study revealed that LTS using the albumin-functionalized PEI membrane was able to establish
284 a polymer-blood vessel junction in an area of 0.25 cm² whose shear strength corresponded to 15%
285 of the shear strength of the native blood vessel. On the basis of an outer diameter of the thoracic
286 artery of about 1.3 mm [17] it can be calculated that a length of an overlapping zone of 4.1 mm,
287 which would span around the entire circumference of the blood vessel, could theoretically provide
288 a shear strength of the PEI-blood vessel compound which would be identical to that of the native
289 blood vessel.

290 The efficacy of the laser welding process is strongly dependent on the structure of the proteins
291 which are used as soldering substrate. For this reason, PEI membrane functionalization with
292 albumin was performed at a physiological pH of 7.4, and not at the commonly used alkaline pH
293 range from 9-12, which favors protein deprotonation [11]. In addition, the temperature of the
294 functionalization process was adapted to the need of an unaffected protein structure and set to +40
295 °C, although higher temperatures (e.g. 70 °C) would result in higher rates of amination [18, 19].

296 FT-ATR-IR analysis of the albumin functionalized PEI showed that the time period used for
297 membrane functionalization had a strong impact on the intensity of carrier membrane amination.
298 PEI functionalization with albumin caused an increase of the peaks of the amide I and II bands

299 over time with peak maxima appearing after 960 min. Desorption of non-covalently bound albumin
300 from the surface by a detergent resulted in a reduction of the amine content of the membrane of
301 only 2.5%. This is the reason why it may be assumed that most of the albumin on the PEI
302 membrane was bound by covalent bonding.

303 A significantly decreased advancing contact angle of $\theta_{adv} = 31.5 \pm 2.3^\circ$ associated with a very low
304 contact angle hysteresis of 3° was a further evidence for an effective functionalization of the PEI
305 membrane. AFM investigation revealed an increase in surface roughness after albumin
306 modification associated with a higher heterogeneity in surface topography, which might limit the
307 reproducibility of LTS repaired tissues.

308 LTS induced fusion of the PEI-membrane-bound solder and adjacent tissue resulted in almost
309 amorphous necrotic zones in the tissue characterized by a delineation of collagen fiber bundles
310 and a reduced number of cell nuclei [4, 8]. LTS is not based on covalent binding between proteins
311 of the solder and the adjacent tissue [18, 19]. LTS was described to cause heat-induced
312 coagulation, instead, of the structural elements of the tissue through cell necrosis and
313 denaturation. It is a rate process characterized by a linear proportionality to time and an
314 exponential proportionality to temperature [20]. The temperature effect is strongly dependent on
315 the laser absorption by the chromophore ICG. After light absorption, the ICG molecule can partially
316 convert the absorbed energy to fluorescent light that is centered at 830 nm [21]. A further minor
317 part of the absorbed light energy is transferred to ICG triplet T_1 state that can generate reactive
318 oxygen species [22]. About 85% of the absorbed energy can be converted to heat inside the ICG
319 molecule by internal conversion [23]. Therefore, heat generation and heat transfer are the major
320 processes after light absorption by ICG [24]. Since in the study presented ICG concentration on the
321 PEI membrane was not changed, the primary determinant of temperature development in solder
322 and tissue during LTS must have been laser power density.

323 Shear strength of the polymer-tissue compound showed a maximum at a laser power output of 450
324 mW. Higher laser powers can generate higher welding temperatures and deeper zones of protein
325 denaturation as described by Poppas et al. [25] and McNally et al. [4], but they do not coincide
326 necessarily with an elevation of compound shear strength, as laser powers higher than 450 mW
327 resulted in this study in reduced shear strength of the PEI-tissue-compound. The main reasons for
328 this phenomenon are assumed to be the blistered distensions which characterized the solder
329 adjacent tissue if laser powers higher than 450 mW were applied. The size of the blisters increased
330 with increasing laser power, and surpassing a power of 1200 mW the blistering effects resulted in a
331 positive exponential correlation between the necrosis zone and the laser power. This reduced the
332 shear strength to one third (36.3%) of the shear strength which was achieved with a laser power of
333 450 mW.

334

335 **5. CONCLUSION**

336 In summary, the results of this study showed that covalent bonding of liquid albumin solders on a

337 polymer carrier can provide benefits with respect to solder allocation and to cohesive strength
338 between solder and tissue. However, results are based on *in-vitro* tests and were performed in
339 dried tissues. Before the clinical applicability of the method can be assessed, additional research is
340 needed to determine the acute and chronic results under wet conditions and in an appropriate
341 animal model.

342

343 **Acknowledgement**

344 This work was supported by the Helmholtz-Association through programme-oriented funding. The
345 authors acknowledge the experimental assistance of Manuela Keller.

346 This paper is dedicated to the 70th birthday of Prof. Friedrich Jung.

347

348

349 **References**

- 350 1. Zeebregts CJ, et al. Non-suture methods of vascular anastomosis. *Br J Surg.*
351 2003;90(3):261-71.
- 352 2. Wolf-de Jonge IC, Beek JF, Balm R. 25 years of laser assisted vascular anastomosis
353 (LAVA): What have we learned? *Eur J Vasc Endovasc Surg.* 2004;27(5):466-76.
- 354 3. Landsman ML, et al. Light-absorbing properties, stability, and spectral stabilization of
355 indocyanine green. *J Appl Physiol.* 1976;40(4):575-83.
- 356 4. McNally KM, et al. Photothermal effects of laser tissue soldering. *Phys Med Biol.*
357 1999;44(4):983-1002; discussion 2 pages follow.
- 358 5. Owen ER, et al. Observations on the effects of CO₂-laser on rat myocardium. *Microsurgery.*
359 1984;5(3):140-3.
- 360 6. He FC, et al. Assessment of tissue blood flow following small artery welding with an
361 intraluminal dissolvable stent. *Microsurgery.* 1999;19(3):148-52.
- 362 7. Bregy A, et al. Solder doped polycaprolactone scaffold enables reproducible laser tissue
363 soldering. *Lasers in surgery and medicine.* 2008;40(10):716-725.
- 364 8. Sorg BS, McNally KM, Welch AJ. Biodegradable polymer film reinforcement of an
365 indocyanine green-doped liquid albumin solder for laser-assisted incision closure. *Lasers*
366 *Surg Med.* 2000;27(1):73-81.
- 367 9. Schalow EL, Kirsch AJ. Laser tissue soldering: Applications in the genitourinary system.
368 *Curr Urol Rep.* 2003;4(1):56-9.
- 369 10. Braune S, Lange M, Richau K, Lützow K, Weigel T, Jung F, Lendlein A. Interaction of
370 thrombocytes with poly(ether imide): The influence of processing. *Clin Hemorheol*
371 *Microcirc.* 2010; 46(2-3): 239-50.
- 372 11. Neffe AT, von Ruesten-Lange M, Braune S, Luetzow K, Roch T, Richau K, Jung F, Lendlein
373 A. Poly(ethylene glycol) Grafting to Poly(ether imide) Membranes: Influence on Protein
374 Adsorption and Thrombocyte Adhesion. *Macromol Biosci.* 2013;13(12):1720-9.

- 375 12. Neffe AT, von Ruesten-Lange M, Braune S, Lutzow K, Roch T, Richau K, Kruger
376 A, Becherer T, Thunemann AF, Jung F, Haag R, Lendlein A, Multivalent grafting of
377 hyperbranched oligo- and polyglycerols shielding rough membranes to mediate
378 hemocompatibility. *J Mater Chem. B.* 2014;2:3626-3635.
- 379 13. Philipp H, et al. The optical properties of a polyetherimide. *Polymer Engineering & Science.*
380 1989;29(22):1574-1578.
- 381 14. Uchida E, Uyama Y, Ikada Y. Sorption of low-molecular-weight anions into thin polycation
382 layers grafted onto a film. *Langmuir.* 1993;9:1121-1124.
- 383 15. Fenner J, et al., Shear strength of tissue bonds as a function of bonding temperature: A
384 proposed mechanism for laser-assisted tissue welding. *Lasers in Medical Science,*
385 1992;7(1):39-43.
- 386 16. Mulisch M, Welsch U. eds. *Mikroskopische Technik.* 18 ed. 2010, Spectrum: Baltimore.
- 387 17. Hiebl B, et al., Macro- and micromorphometric studies of the vascular structures from the
388 Göttingen Minipig. *Applied Cardiopulmonary Pathophysiology.* 2009;13(4):318-321.
- 389 18. Constantinescu MA, et al., Effect of laser soldering irradiation on covalent bonds of pure
390 collagen. *Lasers Med Sci.* 2007;22(1):10-4.
- 391 19. Bass LS, et al., Changes in type I collagen following laser welding. *Lasers Surg Med.*
392 1992;12(5):500-5.
- 393 20. Moritz AR, Henriques FC. Studies of Thermal Injury: II. The Relative Importance of Time
394 and Surface Temperature in the Causation of Cutaneous Burns. *Am J Pathol.*
395 1947;23(5):695-720.
- 396 21. Shafirstein G, et al., Indocyanine green enhanced near-infrared laser treatment of murine
397 mammary carcinoma. *Int J Cancer.* 2012;130(5):1208-15.
- 398 22. Reindl S, et al., Quantum yield of triplet formation for indocyanine green. *Journal of*
399 *Photochemistry and Photobiology A: Chemistry.* 1997;105(1):65-68.
- 400 23. Philip R, et al., Absorption and fluorescence spectroscopic investigation of indocyanine
401 green. *Journal of Photochemistry and Photobiology A: Chemistry.* 1996;96(1-3):137-148.
- 402 24. Cooper CS, et al., Optimal solder and power density for diode laser tissue soldering (LTS).
403 *Lasers in surgery and medicine* 2001;29(1):53-61.
- 404 25. Poppas DP., et al. Temperature-controlled laser photocoagulation of soft tissue: In vivo
405 evaluation using a tissue welding model. *Lasers in surgery and medicine.* 1996;18(4):335-
406 344.
- 407